Global and Planetary Change 242 (2024) 104591

Contents lists available at ScienceDirect

Global and Planetary Change

journal homepage: www.elsevier.com/locate/gloplacha

Research Article

Global carbon cycle disruption during the latest Pliensbachian (Lower Jurassic) evidenced by simultaneous isotopic depletion in marine and terrestrial carbon pools

C.S. O'Keeffe [a,*], L. Schwark [b], I. Bull [c], H.L. Whelton [c], F.L. Gill [a], C.T.S. Little [a]

[a] School of Earth and Environment, University of Leeds, Leeds LS2 9JT, UK
[b] Institute of Geosciences, Christian Albrechts University, Kiel 24118, Germany
[c] Organic Geochemistry Unit, School of Chemistry, University of Bristol, Bristol BS8 1TS, UK

ARTICLE INFO

Editor: Dr. Maoyan Zhu

Keywords:
Isotope geochemistry
Toarcian
Carbon cycle
Jurassic
Cleveland Basin
Black shales

ABSTRACT

The Pliensbachian-Toarcian (Pl-To) boundary was marked by an extinction event in marine organisms, and localised ocean anoxia – resulting in the deposition of black shales. Negative isotopic excursions in bulk organic carbon in many of these black shales, are widely believed to indicate that a global carbon cycle disruption accompanied this extinction event. The Pl-To preceded a period of more intense global carbon cycle disruption that occurred during the Toarcian Oceanic Anoxic Event (T-OAE) by around a million years. It is evident from targeted carbon isotopic analyses of marine and terrestrial organic matter that simultaneous disruptions to the marine and terrestrial carbon cycles occurred during the T-OAE. However, it remains a matter of debate whether the main source of carbon emissions was a climate-sensitive methane reservoir, or volcanic processes. No records of terrestrial carbon cycle disruption exist for the latest Pliensbachian, and so the causal mechanisms behind localised anoxia in this stage of the Lower Jurassic are poorly constrained. We present a record of concomitant isotopic depletion in short and long-chain *n*-alkanes derived from a thin black shale (the Lower Sulphur Band – LSB) deposited during the latest Pliensbachian (located in Yorkshire, UK). A key argument is that simultaneous isotopic depletions in these different compound classes implies the presence of a brief global hyperthermal event in the latest Pliensbachian, with a timescale too short to have been captured by previous analyses of the Yorkshire section. We discuss the relevance of our data to the stratigraphic record of the Lower Jurassic sediments of Yorkshire, highlighting, in particular, the need for better constraint on the ammonite biostratigraphy of the study section. We further argue that the brief climate disruption that occurred in the latest Pliensbachian made the shallow marine environment vulnerable to the development of more widespread marine anoxia, during the succeeding Toarcian stage.

1. Introduction

1.1. The T-OAE and Pl-To

The early Jurassic period was characterised by instability in global climate (notably between 200 and 175 Ma), with alternating greenhouse and icehouse states, and episodes of widespread oxygen depletion in the shallow marine environment (Pálfy and Smith, 2000; Dera et al., 2011; Korte and Hesselbo, 2011; Suan et al., 2011; van de Schootbrugge et al., 2013; Korte et al., 2015; Gómez et al., 2016; Ruebsam et al., 2019, 2020a). These episodes of oxygen depletion are marked by frequent intervals of increased organic carbon (C_{org}) preservation in shallow marine sediments (Silva et al., 2021), which are also often associated with extinction events of varying severity (Little and Benton, 1995; Dera et al., 2010).

The Pliensbachian stage of the Lower Jurassic was characterised by significantly cooler global temperatures than the preceding Sinemurian, and the following Toarcian stages. This is indicated by the heavier $\delta^{18}O$ of shelly macrofauna recovered from sediments of this age, such as the Cleveland Ironstone Formation (Yorkshire, UK; Korte and Hesselbo, 2011; Korte et al., 2015), and the Rodiles Formation of the Asturian Basin (Northern Spain; Gómez et al., 2016). In addition, the occurrence

* Corresponding author.
E-mail addresses: COKeeffe1@hotmail.co.uk (C.S. O'Keeffe), lorenz.schwark@ifg.uni-kiel.de (L. Schwark), ian.d.bull@bristol.ac.uk (I. Bull), helen.whelton@bristol.ac.uk (H.L. Whelton), f.gill@leeds.ac.uk (F.L. Gill), c.t.s.little@earth.leeds.ac.uk (C.T.S. Little).

https://doi.org/10.1016/j.gloplacha.2024.104591
Received 19 February 2024; Received in revised form 12 August 2024; Accepted 15 September 2024
Available online 17 September 2024

of glendonites in upper Pliensbachian sediments from Germany and Siberia (Suan et al., 2011; Teichert and Luppold, 2013; Merkel and Munnecke, 2023; Rogov et al., 2023) strongly imply that the high latitudes reached temperatures below 4 °C. Episodes of mantle-upwelling induced uplift in the North Sea are likely to have limited circulation of warm ocean waters to the high latitudes during the Pliensbachian and Toarcian (Korte et al., 2015; van de Schootbrugge et al., 2020).

This stage of the Lower Jurassic ended with an extinction event (notably for ammonites) at the Pliensbachian-Toarcian boundary (Pl-To) ca. 184.2 Ma (Little and Benton, 1995; Dera et al., 2010; Caruthers et al., 2013; Vasseur et al., 2021). This event precedes the later Toarcian Oceanic Anoxic Event (T-OAE), by approximately one Myr (based on the best estimate for the base of the Serpentinum Zone; Hesselbo et al., 2020), and has been suggested to be genetically linked to it (Littler et al., 2010). Well characterised C_{org} rich black shale successions associated with the T-OAE include the Posidonia Shale of Southern Germany (Röhl et al., 2001) and the Mulgrave Shale Member of the Whitby Mudstone Formation, in the Cleveland Basin (Yorkshire, UK; Hesselbo and Jenkyns, 1995; Simms et al., 2004; Powell, 2010). A negative excursion in the isotopic signature of the C_{org} content of marine sediments ($\delta^{13}C_{org}$) with a magnitude of ~1.5 ‰ is also associated with the Pl-To (hereafter Pl-To CIE), and is observed at many sites across Europe (Littler et al., 2010; Hesselbo and Pieńkowski, 2011; Percival et al., 2015; Fantasia et al., 2019), the Arctic (Suan et al., 2011), Africa (Bodin et al., 2016), and South America (Fantasia et al., 2018). While there is some doubt as to the level of stratigraphic completeness of this excursion at many sites (Suan et al., 2008, 2011; Bodin et al., 2016, 2023) it is nonetheless likely that this marks a widespread perturbation to the carbon cycle.

The T-OAE was an interval of widespread oxygen depletion in shallow marine ecosystems that occurred ca. 183.16 Ma, in the early Toarcian stage of the early Jurassic (Schlanger and Jenkyns, 1976; Hesselbo et al., 2020). It is associated with a prominent negative $\delta^{13}C_{org}$ excursion of −5 to −6 ‰, lasting 0.5 to 1.5 Myr (hereafter T-OAE CIE; Thibault et al., 2018), and has been tied to a disruption of the global exogenic carbon cycle (Hesselbo et al., 2000; French et al., 2014). The ultimate source of the injected ^{12}C is a matter of debate, with suggestions including methane hydrates (Hesselbo et al., 2000; Kemp et al., 2005; Izumi et al., 2018), thermogenic methane produced by volcanism in the Karoo-Ferrar large igneous province (LIP; McElwain et al., 2005; Svensen et al., 2007; Heimdal et al., 2021), wetlands (Them et al., 2017), and permafrost destabilisation at the close of the icehouse state that characterised the late Pliensbachian (Ruebsam et al., 2019, 2020a).

If indeed the Pl-To (like the later T-OAE) was characterised by global disruption to the surface carbon cycle (as suggested by carbon isotope analyses and earth system modelling; Fleischmann et al., 2022), then it is probable that it was accompanied by a hyperthermal event (Clapham and Renne, 2019). While existing belemnite calcite $\delta^{18}O$ records from the Pl-To of the Cleveland basin do not indicate any major changes in sea-surface temperature (SST) in this region (Korte and Hesselbo, 2011; Korte et al., 2015), it is likely that these datasets do not capture sufficiently high-resolution variability in SST across the stage boundary to rule out a coeval, short, sharp temperature rise. Indeed, organic geochemical analysis of tetraether lipids (GDGTs) recovered from Pliensbachian-Toarcian sequences in southern Spain implies that the Pl-To was accompanied by a temperature anomaly of +5 °C (Ruebsam et al., 2020b). Due to the best available $\delta^{18}O$ datasets for the Cleveland Basin being of lower resolution than this record, and potentially influenced by more factors than SST (e.g. palaeosalinity), it is unclear whether or not the temperature curve of Ruebsam et al. (2020b) is reflected here as well.

A brief interval of CO_2 production (the driver for this hyperthermal event) could have been a consequence of the intrusion of lavas in the Karoo-Ferrar LIP prior to the main phase of eruption (McElwain et al., 2005; Svensen et al., 2007). However, the pCO_2 level predicted by purely volcanogenic $\delta^{13}C$ does not agree with pCO_2 reconstructions using leaf stomata data recovered from pre – T-OAE CIE sediments (Ruebsam et al., 2020a). It is more likely that any pCO_2 increase during the Pl-To would have been due to the destabilisation of a climatically sensitive methane reservoir (e.g. Kemp et al., 2005; Them et al., 2017; Ruebsam et al., 2019). The 100-kyr short eccentricity signal observed in $\delta^{13}C_{org}$ records from the lower Jurassic further implies this (Huang and Hesselbo, 2014; Ait-Itto et al., 2018; Ruebsam et al., 2019; Storm et al., 2020).

1.2. Limitations of the bulk $\delta^{13}C$ record

Despite the widespread usage of bulk $\delta^{13}C_{org}$ analysis in studies of the Pl-To and T-OAE CIEs, the reliability of $\delta^{13}C_{org}$ as a proxy for exogenic carbon cycle dynamics is sometimes complicated by the presence of multiple carbon pools within the depositional environment, each bearing a distinct $\delta^{13}C$ signature (van de Schootbrugge et al., 2013). If the C_{org} content of a black shale is derived solely from marine matter, then the $\delta^{13}C_{org}$ signal would be equivalent (notwithstanding any effects in the circulation regime of the basin) to that of the primary marine carbon fixers. However, C_{org} derived from different (e.g. terrestrial) sources, was often in sync with a different $\delta^{13}C$ reservoir at the time it formed. If, therefore, land plant material makes a significant contribution to the sediment C_{org}, the resulting $\delta^{13}C_{org}$ signature would be shifted away from the value of marine organic matter (Jasper and Gagosian, 1990). This is compounded by the fact that terrestrial plants fractionate ^{12}C to a greater degree than marine organisms (−20 to −37 ‰ as opposed to −18 to −25 ‰; Popp et al., 1998; Hayes, 2001; Kohn, 2010).

When first discovered in Tethyan systems in Southern Europe (Jenkyns, 1988) the T-OAE CIE was attributed to the localised upwelling of ^{13}C depleted waters (Küspert, 1982; Sælen et al., 1996). However, Sælen et al. (2000) detected isotopic depletion in the C_{29} *n*-alkane (by −28.0 to −32.0 ‰), in the black shales of the Whitby Mudstone Formation, via compound-specific isotopic analysis (CSIA). The wax lipid carbon isotope signature was 0.7–2.1 ‰ lighter than the concomitant bulk organic matter $\delta^{13}C_{org}$ trend and correlated with it ($R^2 = 0.97$). While this was attributed mainly to the preservation of marine organic matter, the C_{29} *n*-alkane (as well as the C_{27} and C_{28} *n*-alkanes) is commonly derived from epicuticular leaf wax (Eglinton and Hamilton, 1967). Since the $\delta^{13}C$ signal of leaf wax cuticles derived from these plants was in near sync with the $\delta^{13}C$ signal of the atmosphere in which the plant grew (notwithstanding an offset of 5–6 ‰; Pancost and Boot, 2004), a targeted $\delta^{13}C$ analysis of marine sediments (containing sufficient terrestrially derived C_{org}) can provide a record of ^{12}C sequestration in the contemporaneous terrestrial environment. In a study of the Whitby Mudstone Formation, and of the upper Bagå Formation (southwestern Bornholm, Denmark), Hesselbo et al. (2000), also found concomitant negative $\delta^{13}C$ excursions in both bulk TOC, and macrofossil wood particles (Jet, in the Whitby Mudstone Formation), strongly implying a wider carbon-cycle influence on the T-OAE CIE. Further CSIA of the Toarcian aged Posidonia Shale (SW Germany) has also revealed simultaneous depletion in short and long chain *n*-alkanes, which have here been interpreted as reflecting the combined effect of an increased terrestrial C_{org} flux, and wider carbon cycle disruption (Schouten et al., 2000; Ajuaba et al., 2022).

1.3. Geological setting and the Lower Sulphur Band

The Lower Jurassic sediments of the Whitby Mudstone Formation (in the Cleveland Basin) consist of laminated and massive, frequently organic carbon (C_{org}) rich mudstone, with frequent calcareous concretions (Hesselbo and Jenkyns, 1995; Simms et al., 2004; Powell, 2010). Three decimeter-scale black shale units within the Grey Shale Member of the Whitby Mudstone Formation, as well as in the Cleveland Ironstone Formation (see the stratigraphic column in Fig. 1) – the "Sulphur Bands" – remain relatively understudied, compared to the isotopically depleted black shales of the Mulgrave Shale Member (Little and Benton, 1995; Sælen et al., 1996, 2000; Hesselbo et al., 2000; Kemp et al., 2005;

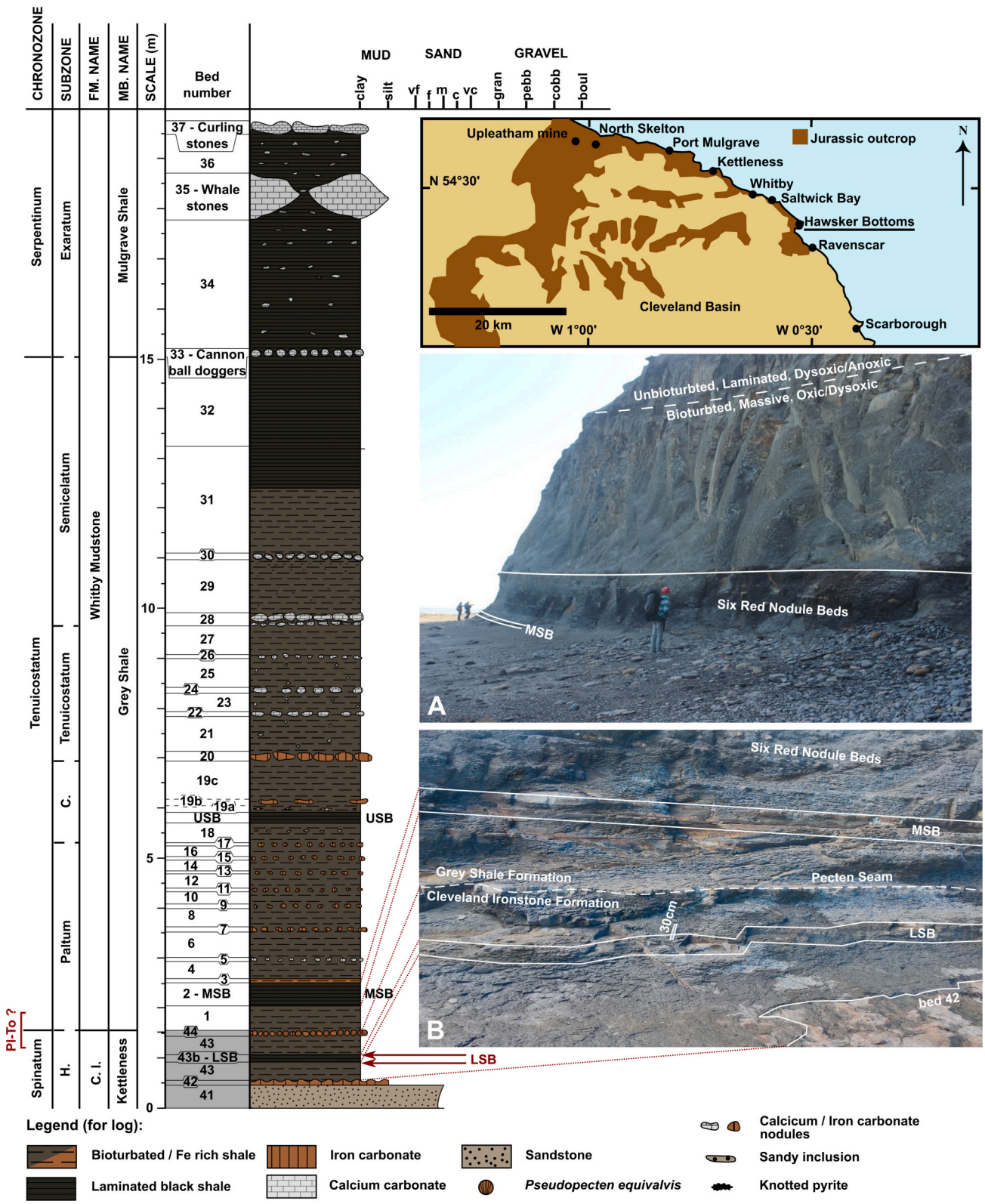

Fig. 1. Map of the study area, with photographs of the sampling locality (54°27′13.27″N, 0°32′3.38″W), and a graphic log of the lower Toarcian mudstones. The LSB and Middle Sulphur Band (MSB) are highlighted in the photographs (along with other stratigraphically important features), and their corresponding positions on the log are indicated. Corresponding bed numbers (from Howarth, 1955, 1973), formation (and member) names and chronozones are also shown to the left of the log, with beds belonging to the Cleveland Ironstone Formation highlighted in grey. The estimated location of the Pl-To (based on Howarth's inference; 1973) within the succession is also indicated. Map adapted from Caswell et al. (2009). Abbreviations of chronozone names: H – Haswskerense; C – Clevelandicum. Abbreviations of formation names: C. I. – Cleveland Ironstone Formation.

Wignall et al., 2005; Danise et al., 2013; French et al., 2014; Slater et al., 2019; Atkinson et al., 2023). The name "Sulphur Bands" is a vernacular term and refers to the sulphureous appearance of these units when weathered, due to their high pyrite content. The ammonite biostratigraphy of the succession (Howarth, 1955, 1973, 1992; Hesselbo and Jenkyns, 1995; Simms et al., 2004) places the upper two Sulphur Bands within the lower Tenuicostatum Zone. The lowest of the three Sulphur Bands – the Lower Sulphur

Band (hereafter LSB) – is 0.15 m thick, and a unit of the Cleveland Ironstone Formation (Spinatum Zone, Hawskerense Subzone; Howarth, 1955; Simms et al., 2004, pp. 265; 267; but see below). The processes responsible for the formation of this unit may foreshadow the later development of more extensive black shale deposition (in the Mulgrave Shale Member), and the widespread extinctions in the benthic community associated with the T-OAE (Little and Benton, 1995; Danise et al., 2013; Atkinson et al., 2023). Given its position in the stratigraphy of the Cleveland Basin, it is probable that the LSB is equivalent to the Organic Matter Preservation Interval (OMPI) associated with the Pl-To (OMPI P-Toa) of Silva et al. (2021).

Littler et al. (2010), reported two $\delta^{13}C_{org}$ excursions in the upper Spinatum, and lower Tenuicostatum zones (an interval encompassing the LSB), reaching −28.5 ‰, and − 27.8 ‰, respectively. Limited $\delta^{13}C$ data derived from macrofossil wood corroborated the observed trend. By comparison of the $\delta^{13}C_{org}$ profile to a similar dataset from Peniche (Portugal; Hesselbo et al., 2007, see section 4), it was suggested that the excursions were caused by an event that affected at least the western European Epicontinental Seaway (EES), and that the excursion might serve as a stratigraphic marker for the Pl-To boundary (see discussion). Precise correlation of the LSB with the Pl-To, is however hampered by alternative placements of the first appearance datum (FAD) of *Dactylioceras (Eodactylites) pseudocommune* within the Cleveland Basin. *D. pseudocommune* appears together with *Dactylioceras (Eodactylites) simplex* at the GSSP for the Toarcian stage boundary at Peniche (Portugal; Hesselbo et al., 2020), the FAD of the latter ammonite being the (biostratigraphic) definition of the Pl-To. Precisely determining this boundary in the Cleveland Basin is less straightforward than for European sections (e.g., in Spain and Germany), due to the lower fossil content (Page, 2003), which results in differing estimates in the literature for its stratigraphic height in the section with respect to Howarth's bed numbering system (Howarth, 1955, 1973; Hesselbo and Jenkyns, 1995; Simms et al., 2004 pp. 265; 267). Crushed specimens of *Dactylioceras* sp. are found in situ in bed 3 of the Grey Shale series (Howarth, 1955), implying that it was deposited during the earliest Toarcian. However, a loose *D. pseudocommune* was recovered from an abandoned ironstone quarry near Saltburn (6.2 km to the SEE of Redcar) by Howarth (1973), and the occurrence of oolitic ironstone on the specimen implies it was reworked from beds 27, or 44, of the Cleveland Ironstone Formation. Based on this find, Hesselbo and Jenkyns (1995), place the base of the Tenuicostatum zone in bed 43 of the Cleveland Ironstone Formation (i.e. the LSB), whereas Simms et al. (2004) retain placement in bed 3 of the Grey Shale Member, based on the lowest known occurrence of in-situ *Dactylioceras* sp.. In lieu of better constraint on the true FAD of *D. pseudocommune*, (or *D. simplex*) we place the Pl-To around bed 44 of the Cleveland Ironstone Formation, following Howarth's inference. However, given that the lowest recorded in-situ *Dactylioceras* sp. are in bed 3, we caution that this placement is provisional, and that it is also possible that the true Pl-To is concomitant with the MSB (rather than the LSB). In addition to underlying the lowest known occurrence of in-situ *Dactylioceras* sp., this unit also has a depleted isotopic signature (Littler et al., 2010), and while the LSB has been correlated to the Pl-To CIE (based on $\delta^{13}C_{org}$ chemostratigraphy; Littler et al., 2010; Boulila and Hinnov, 2017; Thibault et al., 2018; Xu et al., 2018; Fantasia et al., 2019; Ruebsam et al., 2019; Ruebsam and Al-Husseini, 2020), so has the MSB (Al-Suwaidi et al., 2010). In addition to open questions on the biostratigraphy of the sediments encompassing the LSB, assigning a duration with a precision of less than two thousand years to this unit is likely impossible due to the frequent presence of mm-scale hiatuses (Ghadeer and Macquaker, 2011, 2012; Kemp et al., 2018). Nonetheless, rough estimates can be derived using age models based on ammonite biostratigraphy (12.5 Kyr), spectral analysis of the $\delta^{13}C_{org}$ record from the overlying Whitby Mudstone Formation (8–20 Kyr), and inorganic/isotopic geochemistry (5–10 Kyr; see supplementary materials for calculations). We therefore estimate that the LSB was formed over a period of time on the order of 10 Kyr.

While it is widely suggested that the latest Pliensbachian was characterised by a hyperthermal event, and global carbon cycle disruption, the inherently mixed bulk isotopic signatures of many shallow marine successions mean that $\delta^{13}C_{org}$ records alone are not sufficient to support these arguments. While CSIA datasets exist for the T-OAE (Sælen et al., 2000; Schouten et al., 2000; French et al., 2014; Xu et al., 2017; Ruebsam et al., 2020a; Ajuaba et al., 2022), few such records have been evaluated for a unit from the latest Pliensbachian (i.e. Burnaz et al., 2024). Here, we present a CSIA record derived from the LSB. We aim to test whether the $\delta^{13}C_{org}$ excursion of Littler et al. (2010) can be attributed to local water mass changes, a carbon cycle perturbation, or, perhaps, both processes working in concert.

2. Methods

Blocks of the LSB were collected from a wave-cut platform at Hawsker Bottoms (6.28 km to the SW of Whitby; sampling location 54°27′13.27″N, 0°32′3.38"W; see Fig. 1). These were then sampled at a resolution of around two samples per cm for TOC (see supplementary materials). The sample material collected for the CSIA was also used for a complementary organic geochemical analysis (in prep.), which involved a total lipid extraction. This dataset has a sampling resolution of one sample per cm (see supplementary materials for details).

Extraction of the bituminous component of the samples was carried out using a Büchi Speed Extractor E914 pressurized solvent extractor, with a 93:7 mix of DCM and methanol, at 75 °C and at a pressure of 50 bar. Bitumen extracts were separated in an LCTECH automated SPE system into aliphatic, aromatic, and polar fractions via silica gel-column chromatography (6 mL SPE column, 2.8 g Silica 60, 25–40 μm). Aliphatic hydrocarbons were eluted with *n*-hexane. Activated copper turnings were also added to the aliphatic hydrocarbon fraction for the removal of elemental sulphur. The aliphatic fraction was then spiked with two internal standards; A 0.1 mg/g extract of D50 tetracosane (for quantification of acyclic compounds such as *n*-alkanes and isoprenoids), and a 0.025 mg/g extract of D4 cholestane (for quantification of cyclic compounds such as hopanes and steranes).

Gas chromatograph mass spectrometry (GC–MS) analysis of the aliphatic fraction was performed on an Agilent 7890 gas chromatograph (GC) coupled to a Chromtech Evolution mass spectrometer (MS). The GC was fitted with a DB-1MS capillary column (Agilent DB1-HT; 30 m length, 0.25 mm inner diameter, 0.25 μm film thickness), and helium was used as the carrier gas (flow rate of 1.2 mL/min). Aliphatic hydrocarbons were constituted to a concentration of 1 mg/mL, and 1 μL was injected by a COMBI PAL liquid autosampler into a split/splitless injector operated in splitless mode at a temperature of 310 °C. The GC oven temperature program used was: a 5-min isothermal hold at 70 °C, followed by a 10 °C/min increase to 140 °C, then a 3 °C/min increase to 325 °C, and finally a 15-min isothermal hold at 325 °C. The MS was operated in EI mode with an ionization energy of 70 eV and a scanning range from 50 to 600 Da. The ion source was maintained at 300 °C and the transfer line at 320 °C. The quadrupole mass spectrometer was operating in full scan mode from 50 to 750 Da at an energy of 70 eV. Integration of peak areas from the resulting chromatograms was carried using the Agilent Chemstation software (version E.02.02.1431), and the Agilent Masshunter software, for verification of compound identifications and peak area data. No co-elution with the *n*-alkanes of interest was detected, and so the untreated aliphatic fractions were selected for CSIA.

Aliphatic fractions, were evaluated via gas chromatography combustion isotope ratio mass spectrometry (GC-C-IRMS). This analysis was conducted using an Agilent Industries 7890A gas chromatograph coupled to an IsoPrime 100 mass spectrometer. Samples were introduced via a split/splitless injector in splitless mode (purge time 2, purge flow 15) onto a 50 m × 0.32 mm fused silica capillary column coated with a HP-1 stationary phase (100 % polysiloxane, Agilent, 0.17 μm). The GC oven temperature program was set to hold at 50 °C for 2 min, followed by a gradient increase to 300 °C at 5 °C min^{-1} followed by an isothermal hold for 10 min. Helium was used as a carrier gas and maintained at a constant flow of 2 mL min^{-1}. The combustion chamber was maintained at 850 °C, and consisted of a quartz tube packed with copper oxide pellets. An external FAME standard mixture (C_{11}, C_{13}, C_{16}, C_{21}, and C_{23}), of known isotopic composition was included in the runs. $\delta^{13}C$ values are determined from the $^{12}C/^{13}C$ data, as compared with the Vienna Pee Dee Belemnite (VPDB), and calibrated against a CO_2 reference gas of known isotopic composition. Instrument error was ±0.3 ‰, and greater than the variability of replicate analyses. Data processing was carried out using the Ion Vantage software (version 1.6.1.0 IsoPrime).

3. Results

Total Organic Carbon (TOC) increases in the LSB from 0.88 to 6.71 wt% to 4.67–8.36 wt% (with the exception of a decrease to near zero concomitant with a silty lamina at 60 mm; Fig. 2). A suite of *n*-alkanes from *n*-C_{12} to *n*-C_{40} were identified in the LSB, along with pristane and phytane (see Figs. 3 and S1 for representative chromatograms). Both hopanes and steranes also contribute to the aliphatic fraction, with hopanes being much more abundant than steranes (Fig. 3). The *n*-alkanes are far more abundant than both hopanes and steranes, and none of the *n*-alkanes of interest show co-elution with cyclic aliphatic hydrocarbons. The $\delta^{13}C$ values of both short and long-chain *n*-alkanes are lower than the $\delta^{13}C$ values of both bulk TOC ($\Delta\delta^{13}C$ 6–10 ‰). Compound-specific $\delta^{13}C$ values of *n*-alkanes in the upper Grey Shale and Mulgrave Shale Members, which have been attributed to exogenic carbon cycle perturbation (French et al., 2014), exhibit a $\Delta\delta^{13}C$ of 2–6 ‰ (Fig. 4). The long-chain *n*-alkane ^{13}C values are also consistently lower than concomitant $\delta^{13}C_{org}$ of bulk organic matter (Littler et al., 2010) by 3.3–10.6 ‰ (Fig. 2)

4. Discussion

4.1. Isotopic depletion in terrestrial carbon pools

Littler et al. (2010) noted in their discussion of the bulk $\delta^{13}C_{org}$ record from Hawsker Bottoms that this proxy record may reflect both changes in the carbon isotopic composition of the atmosphere, and the relative contribution of different organic matter types to the sedimentary organic matter pool. They suggested that the isotopic composition of the most organic matter rich intervals of the Cleveland Ironstone Formation, and Grey Shale Member of the Whitby Mudstone Formation, may be further investigated, to better constrain these factors – a goal which our work achieves. Our CSIA data of short and long chain *n*-alkanes implies that during the deposition of the LSB, both the marine and terrestrial carbon pools were isotopically depleted (Fig. 2). While vital effects may have played a role in setting the $\delta^{13}C$ of the long chain *n*-alkanes, it is probable that the changing isotopic composition of the atmosphere was the more important factor. Under persistently arid, or fluctuating wet/arid conditions, the $\delta^{13}C$ of C3 plant tissues is positively shifted from the atmospheric value (Kohn, 2010; Schubert and Jahren, 2012; Cernusak et al., 2013), and a decline in the $\delta^{13}C$ signature of *n*-alkanes derived from leaf wax cuticle could therefore reflect a shift to a more humid climate at constant pCO_2 levels (Kohn, 2010). However, analysis of the distribution of fossil leaf types, combined with the distribution of climatically sensitive lithologies (e.g. coal, evaporites) implies that the northern EES was relatively humid for most of the lower Jurassic (Rees et al., 2000), and so changes in the $\delta^{13}C$ signature of leaf wax cuticles are likely to mainly reflect changes in other palaeoenvironmental variables. Humid climate shifts in the geological past are also frequently associated with elevated pCO_2 levels (e.g., the Carnian Pluvial Event; Dal Corso et al., 2011), and if such high pCO_2 levels are the result of depleted carbon release, a decline in the $\delta^{13}C$ of leaf wax cuticle would reflect the influence of two linked palaeoenvironmental changes (humidity and high pCO_2). Furthermore, the effect of elevated atmospheric pCO_2 on plant $\delta^{13}C$ is more pronounced in gymnosperms than in angiosperms and terrestrial animals, and of greater magnitude than the effect of precipitation change (Hare et al., 2018). Given that angiosperms were (probably) absent in the Toarcian (Bateman, 2020; Sauquet et al., 2022), and the assumption that the contribution of terrestrial animal-derived *n*-alkanes to the aliphatic fraction is low, $\delta^{13}C$

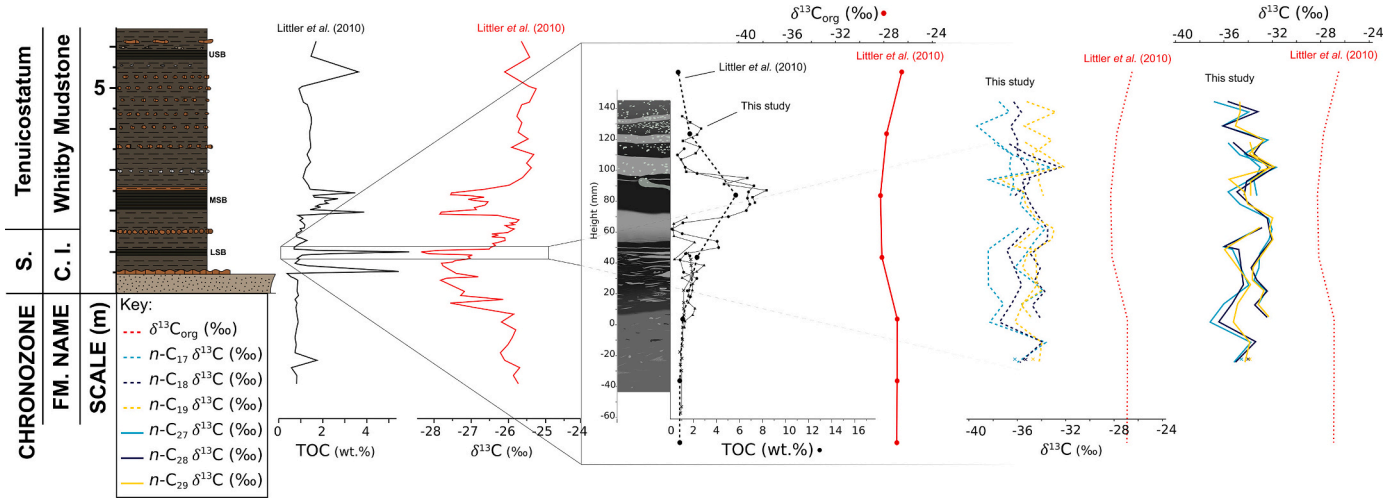

Fig. 2. CSIA dataset compared with the published $\delta^{13}C_{org}$ record from the Cleveland Basin (Littler et al., 2010). The corresponding TOC values for these samples are also plotted (superimposed in our TOC dataset in the LSB). Black lines represent the TOC trends (both ours and that of Littler et al.), and red lines represent the $\delta^{13}C_{org}$ trend of Littler et al. (2010). Dashed lines in other colours represent the up-section trend of lighter carbon-specific isotopic values ($C_{17–19}$), and solid lines represent the trend of heavier values ($C_{27–29}$). A simplified stratigraphic column is also included on the far left. In the plot of our TOC data, circles indicate samples taken from the block coded LSB1, crosses from LSB3, boxes from LSB5, and triangles from LSB6. Abbreviations; S. - Spinatum, C. I. - Cleveland Ironstone. (For interpretation of the references to colour in this figure legend, the reader is referred to the web version of this article.)

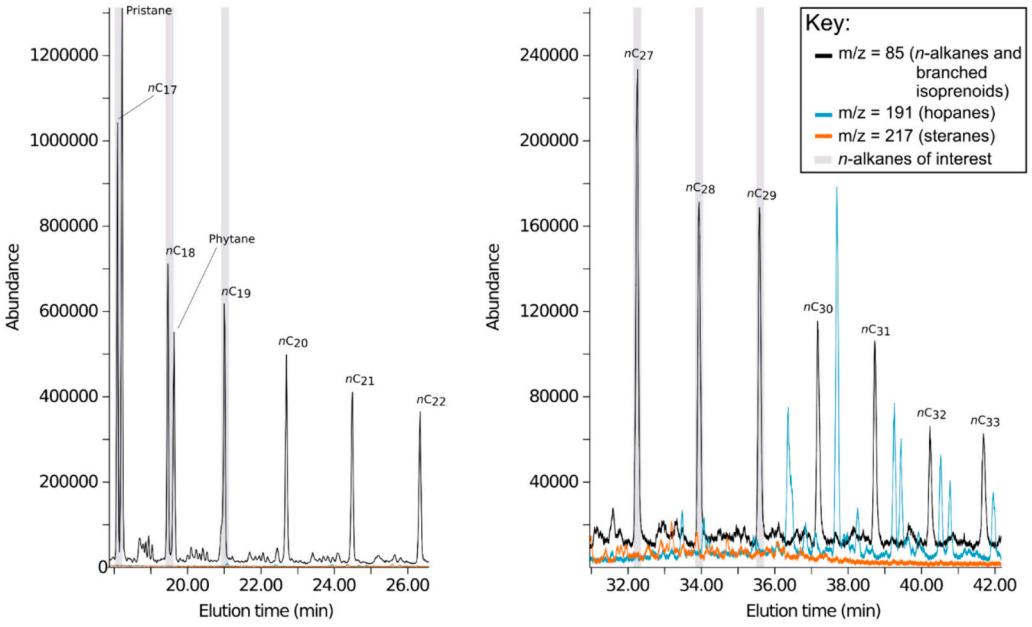

Fig. 3. Gas Chromatography-Mass spectrometry (GC–MS) traces of total ion currect (left) and characteristic mass fragments (right) from a representative aliphatic fraction derived from the LSB (LSB1.8B) with the *n*-alkanes of interest indicated. Note the absence of co-elution *n*-alkanes ($m/z = 85$, black trace) with either hopanes (m/z = 191, blue trace), or steranes (m/z = 217, orange trace). (For interpretation of the references to colour in this figure legend, the reader is referred to the web version of this article.)

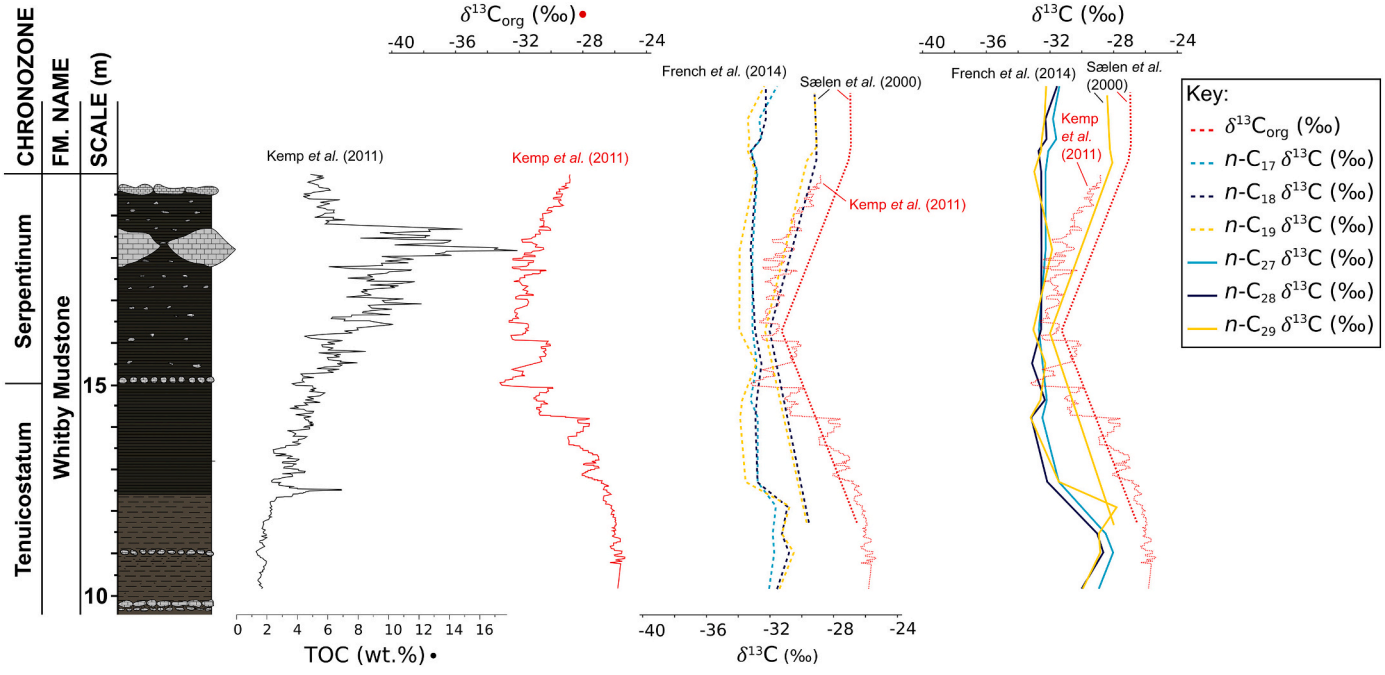

Fig. 4. A comparison of published TOC, $\delta^{13}C_{org}$, and CSIA datasets for the uppermost Grey Shale and Mulgrave Shale Members of the Whitby Mudstone Formation. The same colour scheme used in Fig. 2 is applied here, and the reader is referred to this figure for the key.

of long-chain *n*-alkanes in the sample can be taken as roughly equivalent to the $\delta^{13}C$ of gymnosperm-derived organic carbon. Consequently, we argue that the $\delta^{13}C$ of long-chain *n*-alkanes in our samples is a function of atmospheric (depleted) carbon injection.

It is possible that migration of short chain *n*-alkanes occurred within the sediment pore space, given that the section is comprised of subaerially exposed oil-prone black shales. The sediments of the Hawsker Bottoms section have moderate thermal maturity (with T_{max} values between 431 and 439; Sælen et al., 2000), and free oil is sometimes observed within the Serpentinum Zone (e.g. within ammonites from the Cannon Ball Doggers). However, the TOC content of the LSB is lower than that of the black shales of the Serpentinum Zone by 4–11 wt% (compare Figs. 2, 4), and the up-section distribution of *n*-alkanes per μg of sediment does not deviate greatly from that of TOC (see regression analysis in Fig. 5). So, while it is probable that post-depositional migration occurred (especially with the lighter *n*-alkanes), we suggest that it only effected the up-section variability of the CSIA data, and that the light isotope values still reflect isotopic depletion in the long-chain *n*-

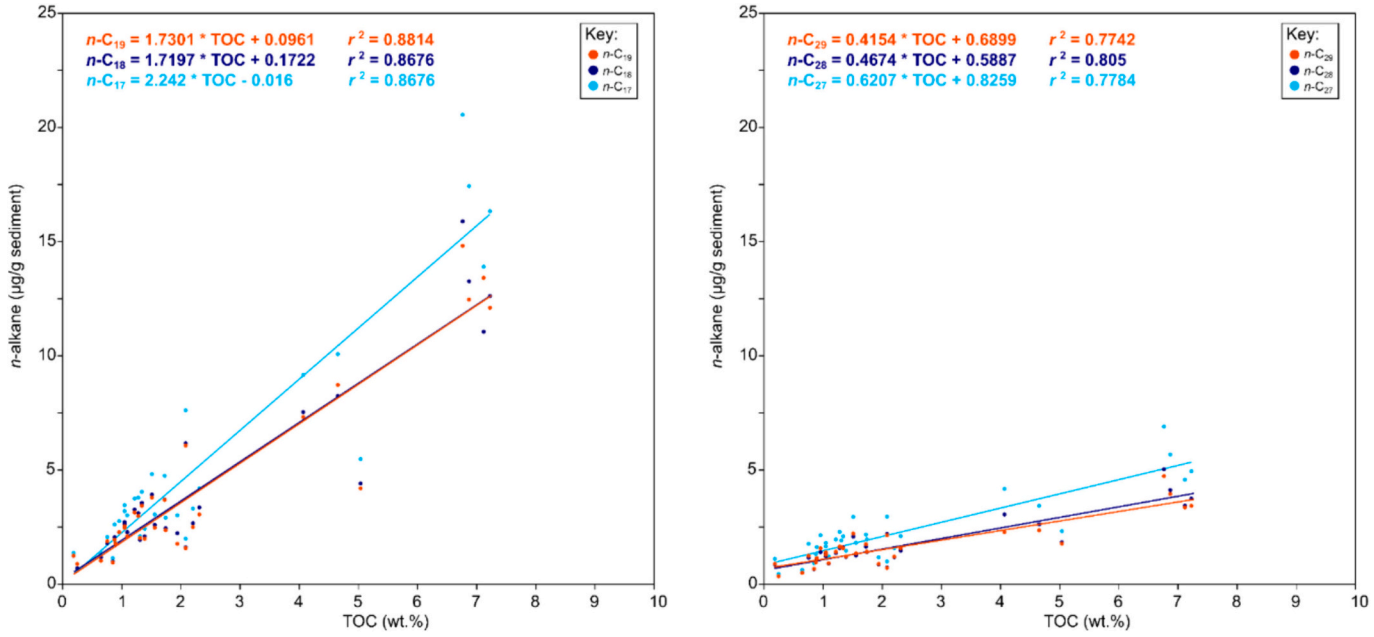

Fig. 5. Regression plots of *n*-alkane content through the sample interval versus the nearest TOC value. The left plot is for *n*-$C_{17–19}$, and the left plot shows the trends for *n*-$C_{27–29}$. Regression equations and corresponding R^2 values are shown for each line (see also supplementary data).

alkanes prior to deposition.

Although we demonstrate synchronous isotopic depletion in marine and terrestrial carbon pools, our sampling methodology is highly stratigraphically constrained, focusing only on the LSB (i.e., prioritizing resolution over completeness). The fact that large jumps in the up-section $\delta^{13}C$ trends were not observed is probably due to this methodology, and it is possible that if our sampling interval is extended further down or up, different $\delta^{13}C$ values could be encountered. This means that our up- section plots of specific isotopic signatures are difficult to place in a wider stratigraphic context. However, our data are nonetheless collected from a unit in the uppermost Pliensbachian, and its deposition was likely soon followed by the Pl-To event (based on the biostratigraphy of the basin; Howarth, 1973; Hesselbo and Jenkyns, 1995). The fact that simultaneous isotopic depletion in marine and terrestrial *n*-alkanes is observed within the LSB (Fig. 2), strongly ties the causal factors behind this short (~10 kyr) period of oxygen depletion to global carbon cycle disruption. This could be related to the Pl-To event, or possibly the late Pliensbachian Spinatum negative event (de Lena et al., 2019; Mercuzot et al., 2019; Storm et al., 2020) - although Howarth's (1973) inferred biostratigraphy implies the former. It is also likely that the Spinatum negative event was triggered by the recycling of ^{13}C depleted water masses (and potentially the remineralisation of sedimentary C_{org}) by enhanced ocean circulation during the late Pliensbachian Icehouse (Mercuzot et al., 2019; Storm et al., 2020). Inorganic geochemical markers such as Mn enrichment imply, by contrast, that the LSB was deposited under highly restricted and stratified conditions, (McArthur et al., 2008; McArthur, 2019).

If the marine environment was strongly stratified (as suggested by the occurrence of high TOC values, and Mn enrichment), then primary producers in the photic zone would have acquired the carbon needed to synthesise short-chain ($C_{17–19}$) *n*-alkanes from an isotopically depleted pool recycled from below the chemocline by episodic upwelling. Such a mechanism has been invoked to explain the prominent negative $\delta^{13}C_{org}$ excursion in the Exaratum Subzone (Sælen et al., 1996, 2000), and possibly contributed to the depleted isotopic signatures of the short chain *n*-alkanes (although this model has been questioned; van Breugel et al., 2006a, 2006b). However, the concomitant $\delta^{13}C$ signatures of terrestrial *n*-alkane pools in the LSB are also consistently isotopically depleted with respect to existing bulk $\delta^{13}C$ data (by 3.3–10.6 ‰; Littler et al., 2010; Fig. 2), which indicates that terrestrial primary producers incorporated depleted carbon as well. As argued by Hesselbo et al. (2000), the presence of prominent, concomitant $\delta^{13}C$ excursions in marine and terrestrial carbon reservoirs is highly unlikely to be coincidental, given the network of interactions between the atmosphere, terrestrial and marine ecosystems in the surface carbon cycle.

4.2. Comparison with the Peniche GSSP

The sediments of the upper Cleveland Ironstone and lower Whitby Mudstone Formations can be correlated with the Lemede (which includes the Toarcian GSSP) and Cabo Carvoeiro formations at Peniche, due to common (ammonite) biostratigraphic markers, and similar geometry of the $\delta^{13}C_{org}$ records at these two localities. *D. simplex* occurs together with *D. pseudocommune* at the Peniche GSSP (da Rocha et al., 2016; Hesselbo et al., 2007) – although, as discussed previously, there are currently alternative placements for the FAD of *D. pseudocommune* in the Cleveland Basin. The FAD of *D. pseudocommune* in the Peniche section occurs within bed 15e (da Rocha et al., 2016). This bed is coincident with a negative $\delta^{13}C_{org}$ excursion of −4 ‰, 9.75 m below the −7 ‰ $\delta^{13}C_{org}$ CIE associated with the T-OAE (Fantasia et al., 2019), and coincides with the base of the Polymorphum Zone. Despite the use of different regional ammonite biostratigraphy, the Polymorphum Zone in the Mediterranean is widely accepted as being laterally equivalent to the Tenuicostatum Zone of the subboreal realm (Littler et al., 2010), and the occurrence of the associated ammonite fauna across the northern and southern EES is likely to be near coincidental (Page, 2017). Belemnite (Hesselbo et al., 2007; Littler et al., 2010), brachiopod (Suan et al., 2008), bulk carbonate, macrofossil wood (Hesselbo et al., 2007), and bulk C_{org} (Fantasia et al., 2019) $\delta^{13}C$ records have all been evaluated through the Peniche GSSP, and all show a negative excursion in bed 15e of −2.5 to −4 ‰. However, given that bed 15e represents a lithological transition from micritic carbonate mudstone towards more siliciclastic marlstone (Duarte, 2007; Littler et al., 2010; da Rocha et al., 2016), and evidence for a concomitant carbonate factory collapse linked to ocean acidification (Suan et al., 2010; Müller et al., 2020; Vasseur et al., 2021 – but see Li et al., 2021; Slater et al., 2022), it is possible that the negative $\delta^{13}C_{carb}$ excursion is due in part to the cessation of carbonate production during the Pl-To (Bodin et al., 2016). While a CSIA of *n*-alkanes has

never been conducted for the Peniche GSSP, Hesselbo et al. (2000, 2007), and Littler et al. (2010) argued for an influence of global carbon cycle disruption on the $\delta^{13}C$ records from both Peniche and Yorkshire, based on parallel negative $\delta^{13}C$ excursions observed in macrofossil wood particles (Jet, in the Cleveland Basin). While some workers have suggested that impregnation of macrofossil wood material by isotopically depleted marine C_{org} hampers its accuracy as an accurate marker for ^{12}C injection into the exogenic carbon cycle (Küspert, 1982), the low C_{org} content and low thermal maturity of the sediments of the Peniche section (Fantasia et al., 2019) implies that the influence of these diagenetic effects on the Peniche $\delta^{13}C_{wood}$ record is minimal. Our data from the Hawsker Bottoms section are also strongly indicative of the addition of isotopically depleted carbon to the atmosphere, and furthermore, CSIA of *n*-alkanes circumvents isotopic heterogeneity effects altogether, since heavier, non-marine *n*-alkanes are specifically targeted (Poole et al., 2004).

Despite containing mutually corroborating records of carbon cycle disruption, hiatal surfaces – indicating episodes of sediment bypass – are widespread in sections spanning the Pl-To (Ruebsam and Al-Husseini, 2020; Bodin et al., 2023), due in part to a regressive-transgressive couplet that affected sedimentation in localities across the EES (Hesselbo, 2008). This was likely related to the termination of the Pliensbachian icehouse (Ruebsam and Schwark, 2021). While condensation is recognised in bed 16a of the Peniche section (Hesselbo et al., 2020; Bodin et al., 2023), given that it does not encompass the defined boundary in bed 15e, nor the FADs of *D. simplex* and *D. pseudocommune*, da Rocha et al. (2016) determined that bed 15e can still be considered the GSSP for the Toarcian. Cryptic hiatal surfaces are recognised in the Cleveland Basin record as well (Ghadeer and Macquaker, 2011, 2012; Kemp et al., 2018; Bodin et al., 2023), and the frequent occurrence of scour marks and cross-stratification within the sedimentary texture of the LSB (Wignall, 1994, p. 92) imply that our record is also likely affected by these. However, the significance of the record of depleted isotopic signatures of terrestrial organic matter that we present here is not diminished by this fact. It is likely that disruption to the global carbon cycle occurred during the deposition of the LSB, regardless of whether or not the temporal coverage of the record is affected by stratigraphic condensation.

Overall, the simultaneous depletion in marine and terrestrial isotope records that we present here, strongly implies that the LSB is at least a local marker for disruption of the exogenic carbon cycle in the latest Pliensbachian. Furthermore, by comparison with the Peniche GSSP, we speculate that it is possible that the LSB was deposited synchronously with the Pl-To stage boundary – although this interpretation is provisional, and subject to review pending determination of the true level of the FAD of *D. pseudocommune* within the succession. Again, this critical biostratigraphic marker has alternative placements within the Lower Jurassic sediments of the Cleveland Basin. Further macropalaeontological study of the uppermost Cleveland Ironstone Formation, and the lowermost Grey Shale Member of the Whitby Mudstone Formation is arguably needed in order to precisely place the stage boundary, and, therefore, accurately determine the event(s) responsible for the isotopic depletion observed in the LSB.

4.3. Climate change in the latest Pliensbachian

The $\delta^{13}C_{org}$ shifts expressed in the Cleveland Basin (including the minimum of −23.5 ‰ associated with the LSB; Littler et al., 2010) can be correlated with 100 kyr short eccentricity maxima (Ruebsam et al., 2019), and it is, therefore, likely that the destabilisation of a climatically sensitive methane reservoir was responsible for the release of ^{13}C depleted carbon during these events. This does not, however, necessarily rule out an association between volcanic activity, and carbon cycle disruption: a slight temperature rise in the high latitudes would have been required to initiate the destabilisation of climatically sensitive methane reservoirs, and this could have been achieved by volcanic degassing of CO_2 (Caruthers et al., 2013; Percival et al., 2015; Xu et al., 2018; Ruebsam et al., 2020a). It is probable that global temperatures were raised due to volcanogenic carbon emissions from the Karoo-Ferrar LIP (which was active at the time; Pálfy and Smith, 2000; Jourdan et al., 2005; Riley et al., 2016), with the subsequent destabilisation of permafrost (and thereby, the major disruption to global climate) being triggered by orbital forcing (Ruebsam et al., 2019). Although existing SST proxy data for the Cleveland Basin (Korte and Hesselbo, 2011; Korte et al., 2015) do not indicate a marked warming in the latest Pliensbachian – of around 10 Kyr in duration – it is likely that these datasets lack sufficient temporal resolution to capture a hyperthermal event of this length. The nearest two $\delta^{18}O$ samples from the datasets of Korte and Hesselbo (2011) and Korte et al. (2015) undershoot and overshoot the LSB by 0.16 m and 0.45 m, respectively.

While the redox state and biodiversity of the shallow marine environment of the Cleveland Basin recovered relatively quickly following the extinction event associated with the Pl-To (Danise et al., 2013), the Cleveland Basin would witness more widespread anoxia one Myr later (during the T-OAE) together with an extinction of many groups of marine organisms (Little and Benton, 1995; Atkinson et al., 2023). The release of CO_2 in the latest Pliensbachian was shorter lived than that occurring during the T-OAE, with the hyperthermal event probably lasting on the order of 10 kyr (based on our estimate for the duration of the deposition of the LSB), and with carbon emissions likely being due to the destabilisation of climatically-sensitive cryosphere reservoirs. It is possible that during the latest Pliensbachian, CO_2 removal mechanisms such as continental weathering (Percival et al., 2016) and C_{org} burial (Bodin et al., 2023), were able to scale with, and eventually outpace CO_2 injection. Furthermore, it is possible that by the early Toarcian, these CO_2 removal mechanisms were overwhelmed, and therefore, the Earth System was less capable of counteracting the effect of the subsequent release of CO_2 during the T-OAE.

5. Conclusion

During the deposition of the LSB, both marine and terrestrial primary producers obtained their carbon from isotopically depleted reservoirs, indicating isotopic depletion in atmospheric carbon. Despite limitations in the ammonite biostratigraphy of the succession at Hawsker Bottoms, the close association between these two carbon-cycling processes strongly implies that the oxygen depletion responsible for the formation of the LSB was the regional expression of a global climate perturbation in the latest Pliensbachian. It is probable that this perturbation was due to the destabilisation of a climatically sensitive methane reservoir. It is possible that this geologically brief interval of global climate change (lasting on the order of 10 Kyr) limited the capacity of the Earth System to buffer the effect of a longer lasting, and more severe period of carbon emission, one Myr later.

CRediT authorship contribution statement

C.S. O'Keeffe: Writing – review & editing, Writing – original draft, Visualization, Validation, Project administration, Methodology, Investigation, Funding acquisition, Formal analysis, Data curation, Conceptualization. **L. Schwark:** Writing – review & editing, Validation, Supervision, Resources, Project administration, Methodology, Investigation, Formal analysis, Data curation, Conceptualization. **I. Bull:** Writing – review & editing, Supervision, Resources, Project administration, Methodology, Investigation, Data curation. **H.L. Whelton:** Writing – review & editing, Validation, Supervision, Resources, Methodology, Investigation, Data curation. **F.L. Gill:** Writing – review & editing, Validation, Supervision, Resources, Project administration, Funding acquisition, Conceptualization. **C.T.S. Little:** Writing – review & editing, Validation, Supervision, Resources, Project administration, Funding acquisition, Conceptualization.

Declaration of competing interest

The authors declare the following financial interests/personal relationships which may be considered as potential competing interests:

Connor O'Keeffe reports financial support was provided by British Geological Survey. Connor O'Keeffe reports financial support was provided by Natural Environment Research Council. If there are other authors, they declare that they have no known competing financial interests or personal relationships that could have appeared to influence the work reported in this paper.

Data availability

I have shared my data as a supplementary file (.xlsx format), which I attached in the "Attach files" step

Acknowledgments

We would like to thank the National Environmental Isotope Facility, for the award of a NERC "grant-in-kind" that covered the CSIA presented here. This work was also supported by a NERC DTP studentship (reference number: NE/L002574/1) and the British Geological Survey University Funding Initiative (BUFI) PhD studentship (S424). The authors wish to thank NERC for partial funding of the National Environmental Isotope Facility (NEIF; contract no. NE/V003917/1) and NERC (contract no. NE/V003917/1) and the University of Bristol for funding the GC-IRMS capabilities. We also extend thanks to S. P. Hesselbo, R. J. Newton and K. N. Page for helpful comments previous versions of this paper.

Appendix A. Supplementary data

Supplementary data to this article can be found online at https://doi.org/10.1016/j.gloplacha.2024.104591.

References

Ait-Itto, F.-Z., Martinez, M., Price, G.D., Ait Addi, A., 2018. Synchronization of the astronomical time scales in the early Toarcian: a link between anoxia, carbon-cycle perturbation, mass extinction and volcanism. Earth Planet. Sci. Lett. 493, 1–11. https://doi.org/10.1016/j.epsl.2018.04.007.

Ajuaba, S., Sachsenhofer, R.F., Bechtel, A., Galasso, F., Gross, D., Misch, D., Schneebeli-Hermann, E., 2022. Biomarker and compound-specific isotope records across the toarcian cie at the Dormettingen section in SW Germany. Int. J. Earth Sci. 111, 1631–1661. https://doi.org/10.1007/s00531-022-02196-z.

Al-Suwaidi, A.H., Angelozzi, G.N., Baudin, F., Damborenea, S.E., Hesselbo, S.P., Jenkyns, H.C., Manceñido, M.O., Riccardi, A.C., 2010. First record of the early Toarcian oceanic anoxic event from the Southern Hemisphere, Neuquén Basin, Argentina. J. Geol. Soc. Lond. 167, 633–636. https://doi.org/10.1144/0016-76492010-025.

Atkinson, J.W., Little, C.T., Dunhill, A.M., 2023. Long duration of benthic ecological recovery from the early toarcian (early jurassic) mass extinction event in the Cleveland Basin, UK. J. Geol. Soc. 180. https://doi.org/10.1144/jgs2022-126.

Bateman, R.M., 2020. Hunting the snark: the flawed search for Mythical Jurassic angiosperms. J. Exp. Bot. 71, 22–35. https://doi.org/10.1093/jxb/erz411.

Bodin, S., Krencker, F.-N., Kothe, T., Hoffmann, R., Mattioli, E., Heimhofer, U., Kabiri, L., 2016. Perturbation of the carbon cycle during the late pliensbachian – early toarcian: new insight from high-resolution carbon isotope records in Morocco. J. Afr. Earth Sci. 116, 89–104. https://doi.org/10.1016/j.jafrearsci.2015.12.018.

Bodin, S., Fantasia, A., Krencker, F.-N., Nebsbjerg, B., Christiansen, L., Andrieu, S., 2023. More gaps than record! A new look at the Pliensbachian/toarcian boundary event guided by coupled chemo-sequence stratigraphy. Palaeogeogr. Palaeoclimatol. Palaeoecol. 610, 111344. https://doi.org/10.1016/j.palaeo.2022.111344.

Boulila, S., Hinnov, L.A., 2017. A review of tempo and scale of the early jurassic Toarcian OAE: implications for carbon cycle and sea level variations. Newsl. Stratigr. 50, 363–389. https://doi.org/10.1127/nos/2017/0374.

Burnaz, L., Littke, R., Grohmann, S., Erbacher, J., Strauss, H., Amann, F., 2024. Lower jurassic (Pliensbachian–toarcian) marine paleoenvironment in Western Europe: sedimentology, geochemistry and organic petrology of the wells mainzholzen and Wickensen, Hils Syncline, lower saxony basin. Int. J. Earth Sci. https://doi.org/10.1007/s00531-023-02381-8.

Caruthers, A.H., Smith, P.L., Gröcke, D.R., 2013. The pliensbachian–toarcian (early jurassic) extinction, a global multi-phased event. Palaeogeogr. Palaeoclimatol. Palaeoecol. 386, 104–118. https://doi.org/10.1016/j.palaeo.2013.05.010.

Caswell, B.A., Coe, A.L., Cohen, A.S., 2009. New range data for marine invertebrate species across the early toarcian (early jurassic) mass extinction. J. Geol. Soc. Lond. 166, 859–872. https://doi.org/10.1144/0016-76492008-0831.

Cernusak, L.A., Ubierna, N., Winter, K., Holtum, J.A., Marshall, J.D., Farquhar, G.D., 2013. Environmental and physiological determinants of carbon isotope discrimination in terrestrial plants. New Phytol. 200, 950–965. https://doi.org/10.1111/nph.12423.

Clapham, M.E., Renne, P.R., 2019. Flood basalts and mass extinctions. Annu. Rev. Earth Planet. Sci. 47, 275–303. https://doi.org/10.1146/annurev-earth-053018-060136.

da Rocha, R.B., Mattioli, E., Duarte, L.V., Pittet, B., Elmi, S., Mouterde, R., Cabral, M.C., Comas-Rengifo, M.J., Gómez, J.J., Goy, A., Hesselbo, S.P., Jenkyns, H.C., Littler, K., Mailliot, S., Oliveira, L.C., Osete, M.L., Perilli, N., Pinto, S., Ruget, C., Suan, G., 2016. Base of the Toarcian stage of the lower jurassic defined by the Global Boundary Stratotype Section and Point (GSSP) at the Peniche Section (Portugal). Episodes 39, 460–481. https://doi.org/10.18814/epiiugs/2016/v39i3/99741.

Dal Corso, J., Mietto, P., Newton, R.J., Pancost, R.D., Preto, N., Roghi, G., Wignall, P.B., 2011. Discovery of a major negative 13C spike in the Carnian (late triassic) linked to the eruption of Wrangellia Flood Basalts. Geology 40, 79–82. https://doi.org/10.1130/g32473.1.

Danise, S., Twitchett, R.J., Little, C.T., Clémence, M.-E., 2013. The impact of global warming and anoxia on marine benthic community dynamics: an example from the Toarcian (early jurassic). PLoS One 8. https://doi.org/10.1371/journal.pone.0056255.

de Lena, L.F., Taylor, D., Guex, J., Bartolini, A., Adatte, T., van Acken, D., Spangenberg, J.E., Samankassou, E., Vennemann, T., Schaltegger, U., 2019. The driving mechanisms of the carbon cycle perturbations in the late pliensbachian (early jurassic). Sci. Rep. 9. https://doi.org/10.1038/s41598-019-54593-1.

Dera, G., Neige, P., Dommergues, J.-L., Fara, E., Laffont, R., Pellenard, P., 2010. High-resolution dynamics of early Jurassic Marine extinctions: the case of pliensbachian–toarcian ammonites (Cephalopoda). J. Geol. Soc. Lond. 167, 21–33. https://doi.org/10.1144/0016-76492009-068.

Dera, G., Brigaud, B., Monna, F., Laffont, R., Pucéat, E., Deconinck, J.-F., Pellenard, P., Joachimski, M.M., Durlet, C., 2011. Climatic ups and downs in a disturbed jurassic world. Geology 39, 215–218. https://doi.org/10.1130/g31579.1.

Duarte, L.V., 2007. Lithostratigraphy, sequence stratigraphy and depositional setting of the Pliensbachian and Toarcian series in the Lusitanian Basin, Portugal. Ciências da Terra (UNL) 16, 17–23.

Eglinton, G., Hamilton, R.J., 1967. Leaf epicuticular waxes. Science 156, 1322–1335. https://doi.org/10.1126/science.156.3780.1322.

Fantasia, A., Föllmi, K.B., Adatte, T., Bernárdez, E., Spangenberg, J.E., Mattioli, E., 2018. The Toarcian oceanic anoxic event in southwestern Gondwana: an example from the Andean basin, Northern Chile. J. Geol. Soc. Lond. 175, 883–902. https://doi.org/10.1144/jgs2018-008.

Fantasia, A., Adatte, T., Spangenberg, J.E., Font, E., Duarte, L.V., Föllmi, K.B., 2019. Global versus local processes during the Pliensbachian–toarcian transition at the Peniche GSSP, Portugal: a multi-proxy record. Earth Sci. Rev. 198, 102932. https://doi.org/10.1016/j.earscirev.2019.102932.

Fleischmann, S., Picotti, V., Caves Rugenstein, J.K., Cobianchi, M., Bernasconi, S.M., 2022. Effects of the Pliensbachian–toarcian boundary event on carbonate productivity of a Tethyan platform and slope. Paleoceanogr. Paleoclimatol. 37. https://doi.org/10.1029/2021pa004392.

French, K.L., Sepúlveda, J., Trabucho-Alexandre, J., Gröcke, D.R., Summons, R.E., 2014. Organic Geochemistry of the early Toarcian oceanic anoxic event in Hawsker Bottoms, Yorkshire, England. Earth Planet. Sci. Lett. 390, 116–127. https://doi.org/10.1016/j.epsl.2013.12.033.

Ghadeer, S.G., Macquaker, J.H.S., 2011. Sediment transport processes in an ancient mud-dominated succession: a comparison of processes operating in marine offshore settings and anoxic basinal environments. J. Geol. Soc. Lond. 168, 1121–1132. https://doi.org/10.1144/0016-76492010-016.

Ghadeer, S.G., Macquaker, J.H.S., 2012. The role of event beds in the preservation of organic carbon in fine-grained sediments: analyses of the sedimentological processes operating during deposition of the Whitby Mudstone Formation (toarcian, lower jurassic) preserved in Northeast England. Mar. Pet. Geol. 35, 309–320. https://doi.org/10.1016/j.marpetgeo.2012.01.001.

Gómez, J.J., Comas-Rengifo, M.J., Goy, A., 2016. Palaeoclimatic oscillations in the pliensbachian (early jurassic) of the Asturian Basin (Northern Spain). Clim. Past 12, 1199–1214. https://doi.org/10.5194/cp-12-1199-2016.

Hare, V.J., Loftus, E., Jeffrey, A., Ramsey, C.B., 2018. Atmospheric CO2 effect on stable carbon isotope composition of Terrestrial Fossil Archives. Nat. Commun. 9. https://doi.org/10.1038/s41467-017-02691-x.

Hayes, J.M., 2001. Fractionation of carbon and hydrogen isotopes in biosynthetic processes. Rev. Mineral. Geochem. 43, 225–277. https://doi.org/10.2138/gsrmg.43.1.225.

Heimdal, T.H., Goddéris, Y., Jones, M.T., Svensen, H.H., 2021. Assessing the importance of thermogenic degassing from the Karoo Large Igneous Province (lip) in driving Toarcian Carbon Cycle perturbations. Nat. Commun. 12. https://doi.org/10.1038/s41467-021-26467-6.

Hesselbo, S.P., 2008. Sequence stratigraphy and inferred relative sea-level change from the onshore British jurassic. Proc. Geol. Assoc. 119, 19–34. https://doi.org/10.1016/s0016-7878(59)80069-9.

Hesselbo, S.P., Jenkyns, H.C., 1995. A comparison of the Hettangian to Bajocian successions of Dorset and Yorkshire. In: Taylor, P.D. (Ed.), Field Geology of the British Jurassic. Geological Society, London, pp. 105–150.

Hesselbo, S.P., Pieńkowski, G., 2011. Stepwise atmospheric carbon-isotope excursion during the Toarcian Oceanic anoxic event (early jurassic, polish basin). Earth Planet. Sci. Lett. 301, 365–372. https://doi.org/10.1016/j.epsl.2010.11.021.

Hesselbo, S.P., Gröcke, D.R., Jenkyns, H.C., Bjerrum, C.J., Farrimond, P., Morgans Bell, H.S., Green, O.R., 2000. Massive dissociation of gas hydrate during a Jurassic Oceanic anoxic event. Nature 406, 392–395. https://doi.org/10.1038/35019044.
Hesselbo, S.P., Jenkyns, H.C., Duarte, L.V., Oliveira, L.C.V., 2007. Carbon-isotope record of the early jurassic (toarcian) oceanic anoxic event from fossil wood and marine carbonate (Lusitanian Basin, Portugal). Earth Planet. Sci. Lett. 253, 455–470. https://doi.org/10.1016/j.epsl.2006.11.009.
Hesselbo, S.P., Ogg, J.G., Ruhl, M., Hinnov, L.A., Huang, C.J., 2020. The Jurassic Period. In: Ogg, G.M., Schmidtz, M.D., Ogg, James G., Gradstein, F.M. (Eds.), Geologic Time Scale 2020. Elsevier, Amsterdam, pp. 955–1021.
Howarth, M.K., 1955. Domerian of the Yorkshire Coast. Proc. Yorks. Geol. Soc. 30, 147–175. https://doi.org/10.1144/pygs.30.2.147.
Howarth, M.K., 1973. The stratigraphy and ammonite Fauna of the Upper Liassic Grey Shales of the Yorkshire Coast. Bull. Br. Mus. (Nat. Hist.) 24, 237–277.
Howarth, M.K., 1992. The ammonite family Hildoceratidae in the lower jurassic of Britain. Monogr. Palaeontogr. Soc. 146, 107–192. https://doi.org/10.1080/25761900.2022.12131773.
Huang, C., Hesselbo, S.P., 2014. Pacing of the toarcian oceanic anoxic event (early jurassic) from astronomical correlation of marine sections. Gondwana Res. 25, 1348–1356. https://doi.org/10.1016/j.gr.2013.06.023.
Izumi, K., Kemp, D.B., Itamiya, S., Inui, M., 2018. Sedimentary evidence for enhanced hydrological cycling in response to rapid carbon release during the early Toarcian Oceanic anoxic event. Earth Planet. Sci. Lett. 481, 162–170. https://doi.org/10.1016/j.epsl.2017.10.030.
Jasper, J.P., Gagosian, R.B., 1990. The sources and deposition of organic matter in the late quaternary pigmy basin, gulf of mexico. Geochim. Cosmochim. Acta 54, 1117–1132. https://doi.org/10.1016/0016-7037(90)90443-o.
Jenkyns, H.C., 1988. The early toarcian (jurassic) anoxic event; stratigraphic, sedimentary and geochemical evidence. Am. J. Sci. 288, 101–151. https://doi.org/10.2475/ajs.288.2.101.
Jourdan, F., Féraud, G., Bertrand, H., Kampunzu, A.B., Tshoso, G., Watkeys, M.K., Le Gall, B., 2005. Karoo large Igneous Province: Brevity, origin, and relation to mass extinction questioned by new $^{40}Ar/^{39}Ar$ AGE data. Geology 33, 745. https://doi.org/10.1130/g21632.1.
Kemp, D.B., Coe, A.L., Cohen, A.S., Schwark, L., 2005. Astronomical pacing of methane release in the Early Jurassic Period. Nature 437, 396–399. https://doi.org/10.1038/nature04037.
Kemp, D.B., Fraser, W.T., Izumi, K., 2018. Stratigraphic completeness and resolution in an ancient Mudrock succession. Sedimentology 65, 1875–1890. https://doi.org/10.1111/sed.12450.
Kohn, M.J., 2010. Carbon isotope compositions of terrestrial C3 plants as indicators of (paleo)ecology and (paleo)climate. Proc. Natl. Acad. Sci. 107, 19691–19695. https://doi.org/10.1073/pnas.1004933107.
Korte, C., Hesselbo, S.P., 2011. Shallow marine carbon and oxygen isotope and elemental records indicate icehouse-greenhouse cycles during the early jurassic. Paleoceanography 26. https://doi.org/10.1029/2011pa002160.
Korte, C., Hesselbo, S.P., Ullmann, C.V., Dietl, G., Ruhl, M., Schweigert, G., Thibault, N., 2015. Jurassic climate mode governed by Ocean Gateway. Nat. Commun. 6. https://doi.org/10.1038/ncomms10015.
Küspert, W., 1982. Environmental changes during oil shale deposition as deduced from stable isotope ratios. In: Cyclic and Event Stratification. Springer-Verlag, Berlin, pp. 482–501.
Li, Q., McArthur, J.M., Thirlwall, M.F., Turchyn, A.V., Page, K., Bradbury, H.J., Weis, R., Lowry, D., 2021. Testing for ocean acidification during the early Toarcian using Δ44/40CA and δ88/86sr. Chem. Geol. 574, 120228. https://doi.org/10.1016/j.chemgeo.2021.120228.
Little, C.T., Benton, M.J., 1995. Early jurassic mass extinction: a global long-term event. Geology 23, 495. https://doi.org/10.1130/0091-7613(1995)023<0495:ejmeag>2.3.co;2.
Littler, K., Hesselbo, S.P., Jenkyns, H.C., 2010. A carbon-isotope perturbation at the Pliensbachian–toarcian boundary: evidence from the Lias Group, Ne England. Geol. Mag. 147, 181–192. https://doi.org/10.1017/s0016756809990458.
McArthur, J.M., 2019. Early toarcian black shales: a response to an oceanic anoxic event or anoxia in marginal basins? Chem. Geol. 522, 71–83. https://doi.org/10.1016/j.chemgeo.2019.05.028.
McArthur, J.M., Algeo, T.J., van de Schootbrugge, B., Li, Q., Howarth, R.J., 2008. Basinal restriction, Black Shales, Re-Os dating, and the early Toarcian (Jurassic) oceanic anoxic event. Paleoceanography 23. https://doi.org/10.1029/2008pa001607.
McElwain, J.C., Wade-Murphy, J., Hesselbo, S.P., 2005. Changes in carbon dioxide during an oceanic anoxic event linked to intrusion into Gondwana Coals. Nature 435, 479–482. https://doi.org/10.1038/nature03618.
Mercuzot, M., Pellenard, P., Durlet, C., Bougeault, C., Meister, C., Dommergues, J.-L., Thibault, N., Baudin, F., Mathieu, O., Bruneau, L., Huret, E., El Hmidi, K., 2019. Carbon-isotope events during the Pliensbachian (Lower Jurassic) on the African and European margins of the NW Tethyan Realm. Newsl. Stratigr. 53, 41–69. https://doi.org/10.1127/nos/2019/0502.
Merkel, A., Munnecke, A., 2023. Glendonite-bearing concretions from the upper pliensbachian (lower jurassic) of South Germany: indicators for a massive cooling in the European epicontinental sea. Facies 69. https://doi.org/10.1007/s10347-023-00667-6.
Müller, T., Jurikova, H., Gutjahr, M., Tomašových, A., Schlögl, J., Liebetrau, V., Duarte, L.V., Milovský, R., Suan, G., Mattioli, E., Pittet, B., Eisenhauer, A., 2020. Ocean acidification during the early Toarcian extinction event: evidence from boron isotopes in brachiopods. Geology 48, 1184–1188. https://doi.org/10.1130/g47781.1.
Page, K.N., 2003. The lower jurassic of Europe: its subdivision and correlation. Geol. Surv. Denmark Greenland Bull. 1, 21–59. https://doi.org/10.34194/geusb.v1.4646.
Page, K.N., 2017. From Oppel to Callomon (and beyond): building a high-resolution ammonite-based biochronology for the jurassic system. Lethaia 50, 336–355. https://doi.org/10.1111/let.12209.
Pálfy, J., Smith, P.L., 2000. Synchrony between early jurassic extinction, oceanic anoxic event, and the Karoo-Ferrar Flood Basalt Volcanism. Geology 28, 747–750. https://doi.org/10.1130/0091-7613(2000)028<0747:sbejeo>2.3.co;2.
Pancost, R.D., Boot, C.S., 2004. The palaeoclimatic utility of terrestrial biomarkers in marine sediments. Mar. Chem. 92, 239–261. https://doi.org/10.1016/j.marchem.2004.06.029.
Percival, L.M.E., Witt, M.L.I., Mather, T.A., Hermoso, M., Jenkyns, H.C., Hesselbo, S.P., Al-Suwaidi, A.H., Storm, M.S., Xu, W., Ruhl, M., 2015. Globally enhanced mercury deposition during the end-pliensbachian extinction and Toarcian OAE: a link to the Karoo–Ferrar Large Igneous Province. Earth Planet. Sci. Lett. 428, 267–280. https://doi.org/10.1016/j.epsl.2015.06.064.
Percival, L.M.E., Cohen, A.S., Davies, M.K., Dickson, A.J., Hesselbo, S.P., Jenkyns, H.C., Leng, M.J., Mather, T.A., Storm, M.S., Xu, W., 2016. Osmium isotope evidence for two pulses of increased continental weathering linked to early jurassic volcanism and climate change. Geology 44, 759–762. https://doi.org/10.1130/g37997.1.
Poole, I., van Bergen, P.F., Kool, J., Schouten, S., Cantrill, D.J., 2004. Molecular isotopic heterogeneity of fossil organic matter: Implications for $\delta^{13}C_{biomass}$ and $\delta^{13}C_{palaeoatmosphere}$ proxies. Org. Geochem. 35, 1261–1274. https://doi.org/10.1016/j.orggeochem.2004.05.014.
Popp, B.N., Laws, E.A., Bidigare, R.R., Dore, J.E., Hanson, K.L., Wakeham, S.G., 1998. Effect of phytoplankton cell geometry on carbon isotopic fractionation. Geochim. Cosmochim. Acta 62, 69–77. https://doi.org/10.1016/s0016-7037(97)00333-5.
Powell, J.H., 2010. Jurassic sedimentation in the Cleveland Basin: a review. Proc. Yorks. Geol. Soc. 58, 21–72. https://doi.org/10.1144/pygs.58.1.278.
Rees, P.McA, Ziegler, A.M., Valdes, P.J., 2000. 10 - Jurassic phytogeography and climates: New data and model comparisons. In: Huber, B.T., Macleod, K.G., Wing, S.L. (Eds.), Warm Climates in Earth History. Cambridge University Press, pp. 297–318.
Riley, T.R., Flowerdew, M.J., Pankhurst, R.J., Curtis, M.L., Millar, I.L., Fanning, C.M., Whitehouse, M.J., 2016. Early jurassic magmatism on the Antarctic Peninsula and potential correlation with the subcordilleran plutonic belt of Patagonia. J. Geol. Soc. Lond. 174, 365–376. https://doi.org/10.1144/jgs2016-053.
Rogov, M., Ershova, V., Gaina, C., Vereshchagin, O., Vasileva, K., Mikhailova, K., Krylov, A., 2023. Glendonites throughout the phanerozoic. Earth Sci. Rev. 241, 104430. https://doi.org/10.1016/j.earscirev.2023.104430.
Röhl, H.-J., Schmid-Röhl, A., Oschmann, W., Frimmel, A., Schwark, L., 2001. The Posidonia Shale (lower toarcian) of SW-Germany: an oxygen-depleted ecosystem controlled by sea level and Palaeoclimate. Palaeogeogr. Palaeoclimatol. Palaeoecol. 165, 27–52. https://doi.org/10.1016/s0031-0182(00)00152-8.
Ruebsam, W., Al-Husseini, M., 2020. Calibrating the early toarcian (early jurassic) with Stratigraphic Black Holes (SBH). Gondwana Res. 82, 317–336. https://doi.org/10.1016/j.gr.2020.01.011.
Ruebsam, W., Schwark, L., 2021. Impact of a northern-hemispherical cryosphere on late pliensbachian–early toarcian climate and environment evolution. Geol. Soc. Lond. Spec. Publ. 514, 359–385. https://doi.org/10.1144/sp514-2021-11.
Ruebsam, W., Mayer, B., Schwark, L., 2019. Cryosphere carbon dynamics control early toarcian global warming and sea level evolution. Glob. Planet. Chang. 172, 440–453. https://doi.org/10.1016/j.gloplacha.2018.11.003.
Ruebsam, W., Reolid, M., Schwark, L., 2020a. δ13C of terrestrial vegetation records Toarcian CO2 and climate gradients. Sci. Rep. 10. https://doi.org/10.1038/s41598-019-56710-6.
Ruebsam, W., Reolid, M., Sabatino, N., Masetti, D., Schwark, L., 2020b. Molecular paleothermometry of the early Toarcian climate perturbation. Glob. Planet. Chang. 195, 103351. https://doi.org/10.1016/j.gloplacha.2020.103351.
Sælen, G., Doyle, P., Talbot, M.R., 1996. Stable-isotope analyses of belemnite rostra from the Whitby mudstone fm., England: Surface water conditions during deposition of a Marine Black Shale. PALAIOS 11, 97. https://doi.org/10.2307/3515065.
Sælen, G., Tyson, R.V., Telnæs, N., Talbot, M.R., 2000. Contrasting watermass conditions during deposition of the Whitby Mudstone (lower jurassic) and Kimmeridge Clay (upper jurassic) formations, UK. Palaeogeogr. Palaeoclimatol. Palaeoecol. 163, 163–196. https://doi.org/10.1016/s0031-0182(00)00150-4.
Sauquet, H., Ramírez-Barahona, S., Magallón, S., 2022. What is the age of flowering plants? J. Exp. Bot. 73, 3840–3853. https://doi.org/10.1093/jxb/erac130.
Schlanger, S.O., Jenkyns, H.C., 1976. Cretaceous Oceanic Anoxic events: causes and consequences. Netherlands J. Geosci. – Geol. Mijnbouw 55, 179–184.
Schouten, S., Sinninghe Damste, J., Schoell, M., Rijpstra, W.I.C., van Kaam-Peters, H.M.E., 2000. Effects of an oceanic anoxic event on the stable carbon isotopic composition of early toarcian carbon. Am. J. Sci. 300, 1–22. https://doi.org/10.2475/ajs.300.1.1.
Schubert, B.A., Jahren, A.H., 2012. The effect of atmospheric CO2 concentration on carbon isotope fractionation in C3 land plants. Geochim. Cosmochim. Acta 96, 29–43. https://doi.org/10.1016/j.gca.2012.08.003.
Silva, R.L., Duarte, L.V., Wach, G.D., Ruhl, M., Sadki, D., Gómez, J.J., Hesselbo, S.P., Xu, W., O'Connor, D., Rodrigues, B., Filho, J.G.M., 2021. An early jurassic (Sinemurian–toarcian) stratigraphic framework for the occurrence of organic matter preservation intervals (ompis). Earth Sci. Rev. 221, 103780. https://doi.org/10.1016/j.earscirev.2021.103780.
Simms, M.J., Chidlaw, N., Morton, N., Page, K.N., 2004. The Cleveland Basin. In: British Lower Jurassic Stratigraphy. Geological Conservation Review. Joint Nature Conservation Committee, Peterborough (UK), pp. 239–304.

Slater, S.M., Twitchett, R.J., Danise, S., Vajda, V., 2019. Substantial vegetation response to early jurassic global warming with impacts on Oceanic anoxia. Nat. Geosci. 12, 462–467. https://doi.org/10.1038/s41561-019-0349-z.

Slater, S.M., Bown, P., Twitchett, R.J., Danise, S., Vajda, V., 2022. Global record of "ghost" nannofossils reveals plankton resilience to high co2 and warming. Science 376, 853–856. https://doi.org/10.1126/science.abm7330.

Storm, M.S., Hesselbo, S.P., Jenkyns, H.C., Ruhl, M., Ullmann, C.V., Xu, W., Leng, M.J., Riding, J.B., Gorbanenko, O., 2020. Orbital pacing and secular evolution of the Early Jurassic carbon cycle. Proc. Natl. Acad. Sci. 117, 3974–3982. https://doi.org/10.1073/pnas.1912094117.

Suan, G., Mattioli, E., Pittet, B., Mailliot, S., Lécuyer, C., 2008. Evidence for major environmental perturbation prior to and during the Toarcian (early jurassic) oceanic anoxic event from the Lusitanian Basin, Portugal. Paleoceanography 23. https://doi.org/10.1029/2007pa001459.

Suan, G., Mattioli, E., Pittet, B., Lécuyer, C., Suchéras-Marx, B., Duarte, L.V., Philippe, M., Reggiani, L., Martineau, F., 2010. Secular environmental precursors to early Toarcian (Jurassic) extreme climate changes. Earth Planet. Sci. Lett. 290, 448–458. https://doi.org/10.1016/j.epsl.2009.12.047.

Suan, G., Nikitenko, B.L., Rogov, M.A., Baudin, F., Spangenberg, J.E., Knyazev, V.G., Glinskikh, L.A., Goryacheva, A.A., Adatte, T., Riding, J.B., Föllmi, K.B., Pittet, B., Mattioli, E., Lécuyer, C., 2011. Polar record of Early Jurassic massive carbon injection. Earth Planet. Sci. Lett. 312, 102–113. https://doi.org/10.1016/j.epsl.2011.09.050.

Svensen, H., Planke, S., Chevallier, L., Malthe-Sørenssen, A., Corfu, F., Jamtveit, B., 2007. Hydrothermal venting of greenhouse gases triggering early jurassic global warming. Earth Planet. Sci. Lett. 256, 554–566. https://doi.org/10.1016/j.epsl.2007.02.013.

Teichert, B.M.A., Luppold, F.W., 2013. Glendonites from an early jurassic methane seep — climate or methane indicators? Palaeogeogr. Palaeoclimatol. Palaeoecol. 390, 81–93. https://doi.org/10.1016/j.palaeo.2013.03.001.

Them, T.R., Gill, B.C., Caruthers, A.H., Gröcke, D.R., Tulsky, E.T., Martindale, R.C., Poulton, T.P., Smith, P.L., 2017. High-resolution carbon isotope records of the toarcian oceanic anoxic event (early jurassic) from North America and implications for the global drivers of the Toarcian Carbon Cycle. Earth Planet. Sci. Lett. 459, 118–126. https://doi.org/10.1016/j.epsl.2016.11.021.

Thibault, N., Ruhl, M., Ullmann, C.V., Korte, C., Kemp, D.B., Gröcke, D.R., Hesselbo, S.P., 2018. The wider context of the lower Jurassic Toarcian oceanic anoxic event in Yorkshire coastal outcrops, UK. Proc. Geol. Assoc. 129, 372–391. https://doi.org/10.1016/j.pgeola.2017.10.007.

van Breugel, Y., Baas, M., Schouten, S., Mattioli, E., Sinninghe Damsté, J.S., 2006a. Isorenieratane record in black shales from the Paris Basin, France: constraints on recycling of respired co2 as a mechanism for negative carbon isotope shifts during the Toarcian oceanic anoxic event. Paleoceanography 21. https://doi.org/10.1029/2006pa001305.

van Breugel, Y., Sinninghe-Damste, J.S., Paetzel, M., Schouten, S., 2006b. Seasonal variation in the stable carbon isotopic composition of algal lipids in a shallow anoxic fjord: evaluation of the effect of recycling of respired CO_2 on the ^{13}C of organic matter. Am. J. Sci. 306, 367–387. https://doi.org/10.2475/05.2006.03.

van de Schootbrugge, B., Bachan, A., Suan, G., Richoz, S., Payne, J.L., 2013. Microbes, mud and methane: cause and consequence of recurrent early Jurassic anoxia following the end-Triassic mass extinction. Palaeontology 56, 685–709. https://doi.org/10.1111/pala.12034.

van de Schootbrugge, B., Houben, A.J., Ercan, F.E., Verreussel, R., Kerstholt, S., Janssen, N.M., Nikitenko, B., Suan, G., 2020. Enhanced Arctic-Tethys Connectivity ended the Toarcian oceanic anoxic event in NW Europe. Geol. Mag. 157, 1593–1611. https://doi.org/10.1017/s0016756819001262.

Vasseur, R., Lathuilière, B., Lazăr, I., Martindale, R.C., Bodin, S., Durlet, C., 2021. Major coral extinctions during the early toarcian global warming event. Glob. Planet. Chang. 207, 103647. https://doi.org/10.1016/j.gloplacha.2021.103647.

Wignall, P.B., 1994. Transgressive black shales - a stratigraphic enigma. In: Black Shales, Oxford Monographs on Geology and Geophysics. Clarendon Press, Oxford, p. 92.

Wignall Newton, R.J., Little, C.T.S, P.B., 2005. The timing of paleoenvironmental change and cause-and-effect relationships during the early jurassic mass extinction in Europe. Am. J. Sci. 305, 1014–1032. https://doi.org/10.2475/ajs.305.10.1014.

Xu, W., Ruhl, M., Jenkyns, H.C., Hesselbo, S.P., Riding, J.B., Selby, D., Naafs, B.D.A., Weijers, J.W.H., Pancost, R.D., Tegelaar, E.W., Idiz, E.F., 2017. Carbon sequestration in an expanded lake system during the Toarcian Oceanic anoxic event. Nat. Geosci. 10, 129–134. https://doi.org/10.1038/ngeo2871.

Xu, W., Mac Niocaill, C., Ruhl, M., Jenkyns, H.C., Riding, J.B., Hesselbo, S.P., 2018. Magnetostratigraphy of the Toarcian Stage (Lower Jurassic) of the Llanbedr (Mochras Farm) borehole, Wales: basis for a global standard and implications for volcanic forcing of Palaeoenvironmental Change. J. Geol. Soc. Lond. 175, 594–604. https://doi.org/10.1144/jgs2017-120.